Food Science of Animal Resources

ARTICLE

Metabolites of *Latilactobacillus curvatus* BYB3 and Indole Activate Aryl Hydrocarbon Receptor to Attenuate Lipopolysaccharide-Induced Intestinal Barrier Dysfunction

Xing Wang, Cheng Chung Yong, and Sejong Oh*

Division of Animal Science, Chonnam National University, Gwangju 61186, Korea

OPEN ACCESS

*Corresponding author : Sejong Oh
Division of Animal Science, Chonnam
National University, Gwangju 61186, Korea
Tel: +82-62-530-2116
Fax: +82-62-530-2129
E-mail: soh@jnu.ac.kr

*ORCID
Xing Wang
https://orcid.org/0000-0002-0775-9306
Cheng Chung Yong
https://orcid.org/0000-0003-0531-6381
Sejong Oh
https://orcid.org/0000-0002-5870-3038

Abstract   This study aimed to investigate the effects of the metabolites of *Latilactobacillus curvatus* BYB3 and indole-activated aryl hydrocarbon receptor (AhR) to increase the tight junction (TJ) proteins in an *in vitro* model of intestinal inflammation. In a Western blot assay, the metabolites of *L. curvatus* BYB3 reduced the TJ demage in lipoploysaccharide (LPS) stimulated-Caco-2 cells. This reduction was a result of upregulating the expression of TJ-associated proteins and suppressing the nuclear factor-κB signaling. Immunofluorescence images consistently revealed that LPS disrupted and reduced the expression of TJ proteins, while the metabolites of *L. curvatus* BYB3 and indole reversed these alterations. The protective effects of *L. curvatus* BYB3 were observed on the intestinal barrier function when measuring transepithelial electrical resistance. Using high-performance liquid chromatography analysis the metabolites, the indole-3-latic acid and indole-3-acetamide concentrations were found to be 1.73±0.27 mg/L and 0.51±0.39 mg/L, respectively. These findings indicate that the metabolites of *L. curvatus* BYB3 have increasing mRNA expressions of cytochrome P450 1A1 (*CYP1A1*) and AhR, and may thus be applicable for therapy of various inflammatory gut diseases as postbiotics.

Keywords   *Latilactobacillus curvatus* BYB3, aryl hydrocarbon receptor, Caco-2 cells, tight junctions, lipopolysaccharide

Introduction

Intestinal epithelial cells (IECs) with intact tight junctions (TJs) form a barrier between the external environment and the mammalian host (Yu et al., 2018). Normal functioning of the intestinal epithelial barrier is critical for maintaining health (Citi, 2018; Odenwald and Turner, 2017; Turner, 2009). Disruption of TJs and paracellular permeability can promote the entry of molecules and activate the immune system, leading to continuous tissue destruction (Lee, 2015). Hence, maintaining the integrity of the intestinal epithelial barrier is critical for inhibiting the development of gastrointestinal diseases and inflammation (Tlaskalová-Hogenová et al., 2004).

Indole, an interspecies and interkingdom signaling molecule, plays essential roles in bacterial pathogenesis and eukaryotic immunity (Lee et al., 2015). The human intestinal tract is rich in a diverse range of about 10^{14} commensal bacteria, some of which are crucial for nutrient assimilation and benefit the immune system (Tlaskalová-Hogenová et al., 2004). A metabolomic study demonstrated that the production of indoxyl sulfate and the antioxidant indole-3-propionic acid in animal blood depended entirely on enteric bacteria (Wikoff et al., 2009). In addition, indole and its derivatives may influence human diseases, such as bacterial infections, intestinal inflammation, neurological diseases, diabetes, and cancers (Lee et al., 2015).

Multiple protein complexes, which are crucial components of TJs, are located in IECs (Tsukita et al., 2001) and include occludin, claudins, and zonula occludens (ZO). These protein complexes are vital for the maintenance of TJs and permit cytoskeletal regulation of the intestinal barrier integrity (Van Itallie and Anderson, 2006). Pathogens damage the intestinal epithelial barrier, increase intestinal permeability, and induce the development of inflammatory bowel disease (IBD) and necrotizing enterocolitis (NEC; Guo et al., 2015). IBD includes two chronic idiopathic inflammatory diseases, ulcerative colitis, and Crohn's disease (Arrieta et al., 2009). Lipopolysaccharide (LPS) is a harmful antigen that can trigger inflammatory responses in the intestinal tissue and can be detected in the serum of patients with NEC and IBD (Han et al., 2020). Recent studies have identified the association between clinically relevant concentrations (1–10 ng/mL) of LPS and intestinal barrier dysfunction under *in vivo* and *in vitro* conditions (Guo et al., 2013). In our previous study, *Latilactobacillus curvatus* BYB3 decreased the disease activity score of dextran sulfate sodium-induced colitis in a mouse model (Wang et al., 2022). Supplementation with indole or using *Lactobacillus reuteri* with high aryl hydrocarbon receptor (AhR) ligand production can improve some metabolic symptoms (Swimm et al., 2018). Therefore, we hypothesized that *L. curvatus* BYB3 has a similar function. The supernatants of *L. curvatus* BYB3 and the metabolites of *L. curvatus* BYB3+indole ameliorated LPS-induced intestinal barrier dysfunction by upregulating the levels of TJ proteins in Caco-2 cells. These findings illustrated the mechanism underlying the destructive effect of clinically relevant concentrations of LPS on the intestinal epithelial barrier, providing evidence for the clinical application of metabolites of *L. curvatus* BYB3+indole in the treatment of LPS-induced intestinal barrier dysfunction.

The AhR is a ligand-dependent transcription factor that is widely expressed in vertebrates and is involved in numerous biological processes, such as cell proliferation (Xie et al., 2012), apoptosis (Marlowe et al., 2008), differentiation (Xie et al., 2012), and inflammatory response (Neavin et al., 2018). The AhR separates from its molecular chaperone complex and forms a heterodimer with the aryl hydrocarbon nuclear translocator (ARNT) in the nucleus. This AhR-ARNT dimer then binds to the upstream regulatory region of its target genes, such as the cytochrome P450 family 1 genes (*CYP1A1* and *CYP1B1*; Esser and Rannug, 2015). Indoles may have utility as an intervention to limit the decline of barrier integrity and the resulting systemic inflammation that occurs with aging (Powell et al., 2020). Indoles and indole-metabolites secreted by the commensal bacteria have been shown to extend the healthspan of diverse organisms, including *Caenorhabditis elegans*, *Drosophila melanogaster*, and mice. The effects of indole and metabolites on animal heatlthspan were found to be AhR-mediated (Sonowal et al., 2017).

This study was conducted to research the effect of *L. curvatus* BYB3 on the intestinal epithelial barrier of the Caco-2 cells. Furthermore, we investigated the differences in mRNA expression levels of CYP1A1 and AhR in response to the metabolites of *L. curvatus* BYB3 and indole.

Materials and Methods

Materials

LPS derived from *Escherichia coli* O111:B4 was purchased from Sigma-Aldrich (Burlington, MA, USA) and dissolved in

phosphate-buffered saline (PBS) to prepare the stock solutions with concentrations of 1 mg/mL. DL-indole-3-lactic acid (ILA), 3-indoleacetic acid (IAA), indole-3-acetamide (IAM), and indole were purchased from Sigma-Aldrich, and trifluoroacetic acid was procured from Daejung Chemicals and Metals (Siheung, Korea). All reagents were stored as specified by the manufacturer. The following antibodies were used in the study: Zona occludens 1 (ZO-1) antibody (Cat No.21772-1-AP, Proteintech, Chicago, IL, USA), claudin-1 antibody (Cat No. ab211737, Abcam, Cambridge, UK), nuclear factor-kappa B (NF-κB) antibody (sc-372, Santa Cruz Biotechnology, Dallas, TX, USA), p-NF-κB p65 (Cell Signaling Technology, Danvers, MA, USA), β-actin C4 antibody (sc-4778, Santa Cruz Biotechnology, Dallas, TX, USA), secondary R-antibody (Cat. No. A11036, Invitrogen, Waltham, MA, USA), and Westar Supernova (Code.XLS3,0100, Cyanagen, Srl, Bologna, Italy).

Indole test

Twenty-one probiotic candidates (Table 1) were cultivated in MRS medium (Difco^{TM} Lactobacilli MRS broth, BD Diagnostics, Franklin Lakes, NJ, USA) for 24 h at 37°C. Before use, the overnight LABs were diluted to a cell density of 10^7 CFU/mL in MRS broth prior to use. Indole was added at a final concentration of 58.5 mg/mL, and the cells were incubated at 37°C for 24 h. Then samples were centrifuged at 2,719.5×g for 15 min at room temperature. A total of 1 mL of the supernatant was collected and mixed immediately with 0.4 mL of Kovac's reagent to determine the extracellular indole concentration. After the Kovac's reagent was added, the mixture was vortexed to separate the phases. The top phase was collected, and the absorbance was measured at 540 nm.

Bacterial cultivation and cell-free supernatant (CFS) harvesting

L. curvatus BYB3 cells were isolated from traditional homemade kimchi in Gwangju and Jeollanam-do, and maintained in MRS broth. Cells were incubated in the MRS broth at 37°C and centrifuged at 1,500×g for 15 min at room temperature to obtain cell pellets. The pellets were stored in 10% glycerol or skim milk at –80°C until further use. The supernatant was filtered using a 0.2 μm syringe (Sartorius AG, Gottingen, Germany). The cells in the indole group were treated with 58.5 mg/mL indole, those in the BYB3 group were incubated with *L. curvatus* BYB3, and those in the BYB3+indole group were treated with both *L. curvatus* BYB3 and 58.5 mg/mL indole. The three groups were incubated in the MRS medium for 24 h at 37°C. The cell pellets were discarded, and the CFSs were used to treat the Caco-2 cells.

Cell culturing and treatment protocol

The Caco-2 cells used in the study were obtained from the Korean Cell Line Bank (No.30037.1, Seoul, Korea). Caco-2 cells were cultured in Modified Eagles Medium (MEM), high glucose (HyClone Laboratories, Logan, UT, USA), supplemented with 20% fetal bovine serum (Gibco^{TM}, Thermo Fisher Scientific, Waltham, MA, USA), 1% MEM non-essential amino acids solution (100×; Gibco^{TM}, Thermo Fisher Scientific), and 1% antibiotic-antimycotic solution (Gibco^{TM}, Thermo Fisher Scientific) at 37°C in an atmosphere containing 5% CO_2. The medium was replaced every two or three days. The Caco-2 cells ($1×10^6$ cells) were seeded in a 20×90 mm dish and treated with 10 ng/mL of LPS. They were then treated with 1 mL of indole, 1 mL of *L. curvatus* BYB3, and 1 mL of the BYB3+ indole metabolites supernatants.

Transepithelial electrical resistance (TEER) assay

Caco-2 cells ($1×10^3$ cells/cm²) were seeded in a Corning®, Costar®, Transwell® chamber with 0.4 μm pores (Corning, New

Table 1. Probiotic candidates tested

No.	Strains	Abbreviation	Source	Renamed genus (Zheng et al., 2020)
1	*L. curvatus* BYB1	BYB1	Kimchi	*Latilactobacillus curvatus*
2	*L. curvatus* BYB2	BYB2	Kimchi	*Latilactobacillus curvatus*
3	*L. curvatus* BYB3	BYB3	Kimchi	*Latilactobacillus curvatus*
4	*L. curvatus* BYB4	BYB4	Kimchi	*Latilactobacillus curvatus*
5	*L. curvatus* BYB7	BYB7	Kimchi	*Latilactobacillus curvatus*
6	*L. brevis* OB1	OB1	Kimchi	*Levilactobacillus brevis*
7	*L. brevis* OB4	OB4	Kimchi	*Levilactobacillus brevis*
8	*L. brevis* OB3	OB3	Kimchi	*Levilactobacillus brevis*
9	*L. sakei* OB8	OB8	Kimchi	*Latilactobacillus sakei*
10	*L. casei* MYA5	MYA5	Kimchi	*Lacticaseibacillus casei*
11	*L. sakei* JNU533	JNU533	Kimchi	*Latilactobacillus sakei*
12	*L. sakei* MYA6	MYA6	Kimchi	*Latilactobacillus sakei*
13	*L. fermentum* NS4	NS4	Kimchi	*Limosilactobacillus fermentum*
14	*L. amylovorus* CH6	KCNU	Swine intestine	Unchanged
15	*L. acidophilus* GP1B	GP1B	Swine intestine	Unchanged
16	*L. plantarum* L67	L67	Infant feces	*Lactiplantibacillus plantarum*
17	*L. plantarum* OY1	OY1	Kimchi	*Lactiplantibacillus plantarum*
18	*L. plantarum* OY2	OY2	Kimchi	*Lactiplantibacillus plantarum*
19	*L. fermentum* JNU532	JNU532	Kimchi	*Limosilactobacillus fermentum*
20	*L. fermentum* JNU534	JNU534	Kimchi	*Limosilactobacillus fermentum*
21	*L. rhamnosus* GG	LGG	Human intestine	*Latilactobacillus rhamnosus*

York, NY, USA) that had been placed in a 24-well plate. Another Transwell® plate was kept blank. After reaching confluence, the cells were differentiated and polarized for 7–10 days in the culture medium. Subsequently, the Caco-2 cells were treated with 10 ng/mL of LPS and later with 100 µL of indole supernatant, 100 µL of *L. curvatus* BYB3 supernatant, and 100 µL of BYB3+ indole supernatants. The TEER assay was used to measure cell monolayer integrity before and after all treatments. The TEER was measured using an epithelial volt-ohm-meter equipped with a chopstick electrode [Millicell® ERS-2 (Electrical Resistance System), EMD Millipore, Burlington, MA, USA]. The electrode was immersed at a 90° angle, with one tip in the basolateral chamber and the other in the apical chamber. Care was taken to prevent contact of the electrode with the monolayer. Measurements were performed in triplicate for each monolayer. An insert without Caco-2 cells was used as a blank; the mean resistance of the blank was subtracted from all samples. The unit area resistance was calculated by dividing the resistance values by the effective membrane area (0.33 cm^2).

RNA isolation and gene expression analysis

Caco-2 cells (1×10^6 cells) seeded in a 20×90 mm dish were treated with 10 ng/mL of LPS followed by treatment with 1 mL of indole supernatant, 1 mL of strain 3, 15 and LGG supernatant, and 1 mL of indole+strain 3, 15 and LGG supernatants.

After incubation for 24 h, the cells were collected for further analysis. Total RNA was isolated and converted into complementary DNA (cDNA) as described previously. Briefly, 2 μg of total RNA was used to cDNA using a Maxime RT PreMix kit (Oligo Dt primer; Cat. No. 25081, iNtRON Biotechnology, Seongnam, Korea). The following primers were used for real-time polymerase chain reaction (RT-PCR; Table 2).

PCR was performed under the following conditions: Initial denaturation at 94℃ for 3 min, followed by 40 cycles of the program with incubations at 94℃ for 30 s, 60℃ for 30 s, and 72℃ for 1 min, followed by incubation at 65℃ for 5 s, until the end of the program. The relative gene expression levels were determined by comparative analyses using the formula:

$$\text{Relative expression} = 2^{-(\Delta Ct)}, \text{with } \Delta C_t = C_{t\,gene} - C_{t\,GAPDH}$$

Protein extraction and Western blot analysis

Caco-2 cells (1×10^6 cells) were seeded in a 20×90 mm dish and treated with 10 ng/mL of LPS and then 1 mL of the indole supernatant, 1 mL of BYB3 supernatant, and 1 mL of indole+BYB3 metabolites supernatant. After incubation for 24 h, the cells were collected for further analysis.

The total protein concentration in the cell lysates was determined using the PRO-PREP protein extraction solution (iNtRON Biotechnology). Briefly, 5×10^6 cells were immersed in 400 μL of the PRO-PREP solution and homogenized in ice for 10–20 min. The mixture was then centrifuged at 13,000×g at 4℃ for 5 min, and the extracted protein was collected in the supernatant. The protein concentration was determined by the Pierce BCA Protein Assay Kit (Thermo Fisher Scientific). Equal amounts of protein (50 μg per lane) were separated using 10% sodium dodecyl sulfate-polyacrylamide gel, electroblotted (Mini-PROTEAN® II Cell Systems, Bio-Rad Laboratories, Hercules, CA, USA), and transferred to a polyvinylidene difluoride membrane (Bio-Rad Laboratories). The proteins were blocked with 5% skim milk (Difco Laboratories, Detroit, MI, USA) and underwent overnight antibody incubation against E-cadherin, N-cadherin, Vimentin, and β-actin at 4℃. After incubation, the membranes were washed and incubated with horseradish peroxidase-conjugated goat anti-mouse or anti-rabbit antibodies for 1 h at room temperature. After each was washed three times with PBST for 10 min, protein bands developed. The bands were detected via enhanced chemiluminescence, and the band density was determined using β-actin as the reference protein.

Immunofluorescence staining of zona occludens 1 (ZO-1), claudin-1, and nuclear factor-kappa B (NF-κB)

Caco-2 cells were seeded on a 24-well plate at a density of 1×10^3 cells/mL. These cells were treated with 10 ng/mL of LPS

Table 2. Primer sequences for quantitative polymerase chain reaction (PCR)

Gene	Primer sequences	References
CYP1A1	F: TCGGCCACGGAGTTTCTTC	(Yang et al., 2022)
CYP1A1	R: GGTCAGCATGTGCCCAATCA	
AhR	F: CAAATCCTTCCAAGCGGCATA	(Behfarjam and Jadali, 2018)
AhR	R: CGCTGACCTAAGAACTGAAAG	
GAPDH	F: GAAATCCCA CACCATCTTCC	
GAPDH	R: AAATGAGCCCCAGCCTTCT	

CYP, cytochrome P450; AhR, aryl hydrocarbon receptor; GAPDH, glyceraldehyde-3-phosphate dehydrogenase.

and then with 100 µL each of indole, *L. curvatus* BYB3, BYB3+indole metabolite supernatants. After treatment for 24 h, the cells were collected for the next step.

The cells were prepared as described in Material and Methods. Caco-2 cells were grown on glass coverslips; the slides were washed with PBS for 5 min at room temperature, fixed with 3.7% formaldehyde in PBS buffer for 20 min at 4℃, and again rinsed thrice with PBS buffer for 5 min at room temperature. The monolayers were permeabilized with 0.5% Triton™ X-100 (Sigma-Aldrich) for 20 min at room temperature and rinsed three times with PBS buffer for 2 min at room temperature. The slides were blocked with 5% skim milk in tris buffered saline with Tween® (TBST) for 1 h at room temperature without rinsing. They were then incubated with rabbit polyclonal anti-ZO-1 antibody, rabbit monoclonal anti-claudin-1 antibody, and rabbit polyclonal anti-NF-κB p65 antibody for 2 h at room temperature. The slides were rinsed thrice with TBST for 5 min at room temperature. The remaining incubations were performed in the dark. The slides were further incubated with an Alexa Fluor® 568 goat anti-rabbit secondary antibody (Abcam). Nuclei were stained using 4',6-diamidino-2-phenylindole dihydrochloride (DAPI; Cat. No D1306, Invitrogen) for 15 s at room temperature. The samples were covered with a coverslip using the Vectashield® anti-fade mounting medium (Vector cat. #H-1000, Vector Laboratories, Newark, CA, USA). The edges of the coverslips were sealed by nail polishing. The slides were examined and analyzed using a fluorescence microscope (Olympus BX50, Olympus, Tokyo, Japan).

Analysis of the metabolites in the cell-free supernatants (CFSs) by high-performance liquid chromatography (HPLC)

The indole derivatives in the CFSs were analyzed as previously described. Briefly, filtered samples were injected (10 mL), in triplicate, into an HPLC system (KNAUER, Wissenschaftliche Geräte GmbH, Berlin, Germany) equipped with a C-18 gravity 150×4.6 mm column, particle size: 5 µm (Macherey-Nagel GmbH & Co. KG, Düren, Germany). The flow rate was set to 1 mL/min, and the column oven temperature was maintained at 30℃. The running buffers were 0.3% trifluoroacetic acid solutions prepared in ultra-pure water (A) and acetonitrile (B). The process was initiated with an A:B ratio of 90:10; the linear gradient was applied to reach this ratio in 1 min. The steps included gradients with 55% solution A: 45% solution B for 28 min, 5% solution A: 95% solution B for 30 and 35 min, and 90% solution A: 10% solution B for 36 min. The measurements were stopped after 45 min. The detection wavelength was set at 280 nm.

Statistical analysis

All data are presented as mean±SD of triplicate experiments. Statistical significance comparing different sets of groups was determined using the Student's t-test. In experiments comparing multiple experimental groups, statistical differences between groups were analyzed using one-way analysis of variance (ANOVA). Statistical analyses were performed using IBM® SPSS® Statistics 20 (IBM, Chicago, IL, USA), and a $p<0.05$ was considered statistically significant.

Results

Indole test result of the probiotic candidates' cell-free supernatants (CFSs)

The probiotic candidates (Table 1 and Fig. 1) show the *Lactobacillus* strains' ability to metabolize and reduce indole concentration during fermentation. Among the tested *Lactobacillus* strains, 3 (*L. curvatus* BYB3), 15 (*Lactobacillus acidophilus*), and 21 (*Lactilacobacillus rhamnosus* GG) demonstrated remarkable indole reducing abilities and were selected
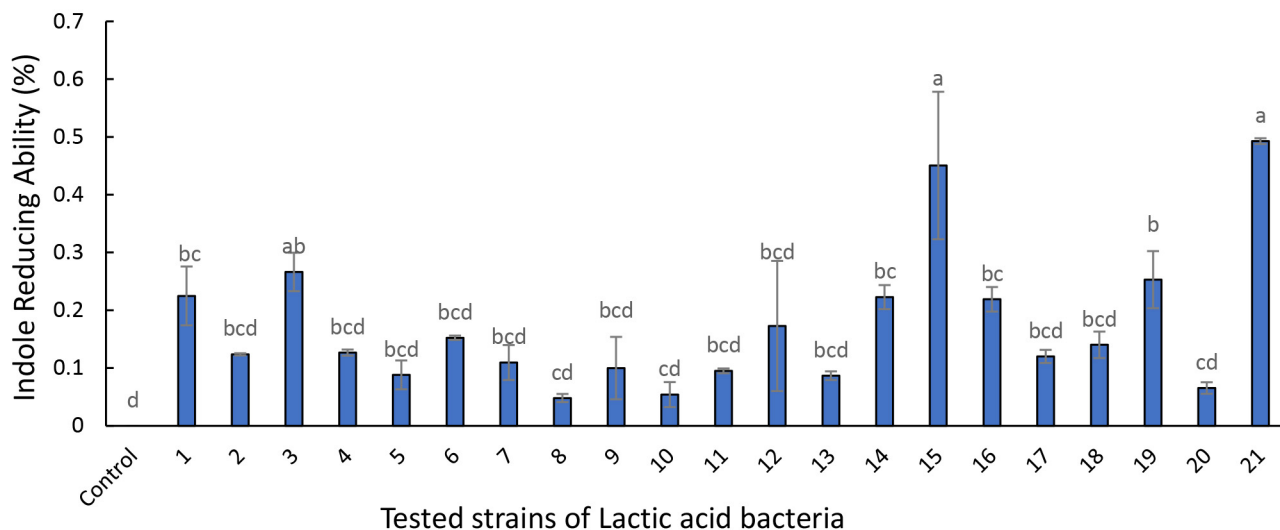
Fig. 1. Indole test results of the probiotic candidates' CFSs. Indole test of 21 candidate strains for examination of metabolism. The mean values of the samples are significantly different (indicated by different letters). Different letters indicate significant differences according to the change in indole concentration from low to high. The values of the experimental groups were normalized to those of the control groups, and statistically significant differences are indicated by * $p<0.05$, ** $p<0.01$. Data are presented as the mean±SD (n=3). CFS, cell-free supernatant.
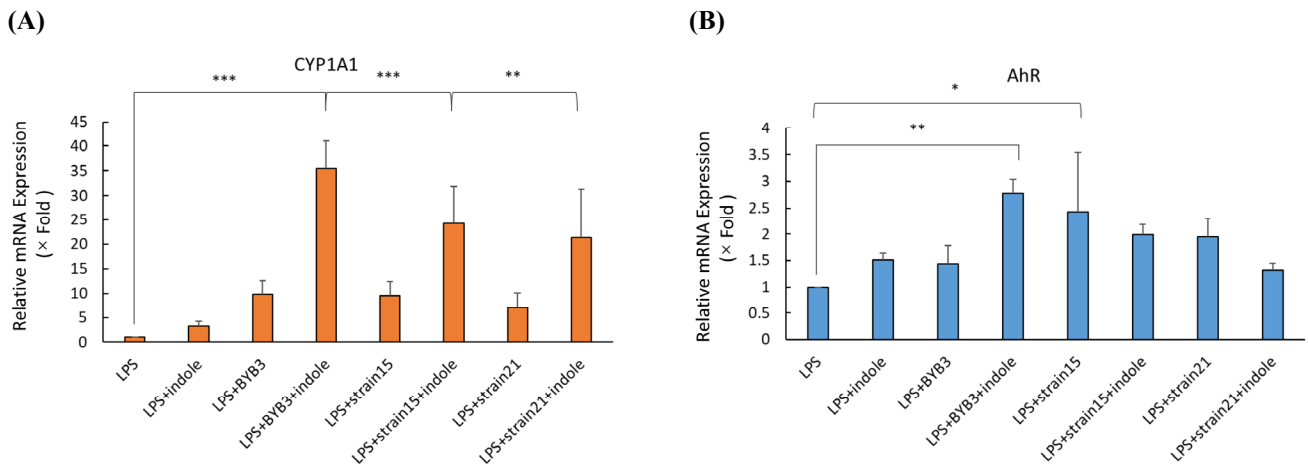
for subsequent analyses.

Metabolites of *Latilactobacillus curvatus* BYB3 and indole significantly increased aryl hydrocarbon receptor (AhR) activation in lipopolysaccharide (LPS)-treated Caco-2 cells

Caco-2 cells were treated with the 10% MRS as the control and 10% supernatant of the strains (3, 15, and 21) previously screened for 24 h. Treatment of the Caco-2 cells with 10 ng/ mL of LPS simulated the conditions of colitis. A previous study detected increased expression of *CYP1A1*, which is indicative of the AhR activation (Yu et al., 2018). To confirm the activation of the AhR by the metabolites, the mRNA expression levels of *CYP1A1* and *AhR* were determined after treating the Caco-2 cells for 24 h with LPS alone or in combination with other supernatants. The supernatants of *L. curvatus* BYB3 and indole significantly increased the mRNA expression *CYP1A1* and *AhR* by 35-fold and 3-fold, respectively (Figs. 2A and B).

Metabolites of *Latilactobacillus curvatus* BYB3 and indole increased the transepithelial electrical resistance (TEER) in lipopolysaccharide (LPS)-induced Caco-2 cells

The TEER was used to measure cell monolayer integrity, which was assessed before and after all treatments. LPS increased the permeability of the intestinal epithelial barrier. However, the effects of the metabolites of *L. curvatus* BYB3 and indole on the LPS-mediated increase in intestinal permeability are unknown. LPS significantly decreased the TEER after 12 h; the reduction continued for 24 h after application (Fig. 3). In contrast, the metabolites of *L. curvatus* BYB3 and indole remarkably increased the TEER. This finding suggests that the metabolites reduced the permeability of the intestinal epithelial barrier. In addition, the supernatants of *L. curvatus* BYB3 and indole increased the TEER. However, co-treatment with the metabolites and LPS significantly restored the LPS-mediated increase in the permeability of the intestinal epithelial barrier in Caco-2 cells (Figs. 2 and 3). Hence, these metabolites could significantly protect against LPS-induced intestinal permeability.

(A)

(B)

Fig. 2. Metabolites of *Latilactobacillus curvatus* BYB3 and indole significantly increased AhR activation in LPS-treated Caco-2 cells. (A, B) Show the mRNA levels of *CYP1A1* and *AhR* in 10 ng/mL LPS-induced cells, respectively. The sample sequence is the control (supernatant of the medium MRS), and supernatants after treatment with indole, *L. curvatus* BYB3, BYB3+indole, strain 15, strain 15+indole, strain 21, strain 21+indole, which were added in turn. Different letters indicate the mean values of the samples that are significantly different according to the changes in mRNA expression. Experimental groups were normalized to control groups; statistically significant differences are shown by * $p < 0.05$ and ** $p < 0.01$. Data are presented as mean±SD (n=3). CYP, cytochrome P450; LPS, lipopolysaccharide; AhR, aryl hydrocarbon receptor.
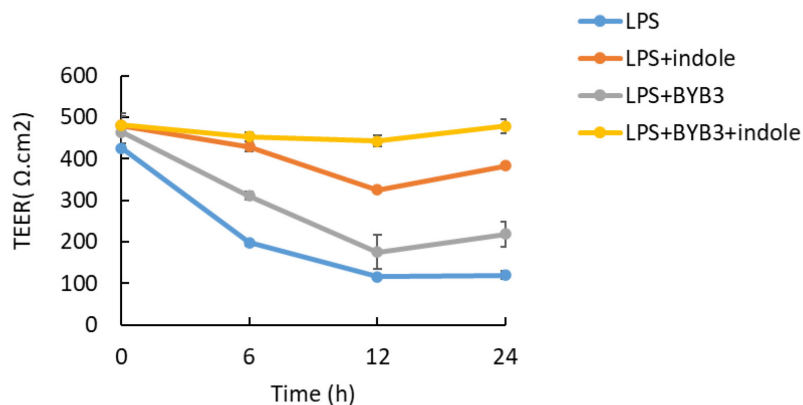

Fig. 3. Metabolites of *Latilactobacillus curvatus* BYB3 and indole increased the TEER in LPS-treated Caco-2 cells. Metabolites of *L. curvatus* BYB3 and indole significantly increased the TEER of Caco-2 cell monolayers in response to an inflammatory stimulus (LPS). After incubation with 10 ng/mL of LPS, the supernatants were incubated with indole, *L. curvatus* BYB3, and BYB3+indole from 0 to 24 h. The data are presented as the mean±SD (n=3). Statistically significant differences are shown by * $p < 0.05$ and ** $p < 0.01$. TEER, transepithelial electrical resistance; LPS, lipopolysaccharide.

Effect of metabolites of *Latilactobacillus curvatus* BYB3 and indole on the expression of tight junction (TJ) proteins and inflammatory responses in Caco-2 cells

LPS down-regulated the expression of the ZO-1, occludin, and claudin-1 proteins. Caco-2 cells were co-treated with 10 ng/mL of LPS, the supernatants of indole and *L. curvatus* BYB3, and the metabolites of BYB3+indole for 24 h to determine alterations in the expression of the TJ proteins. The Caco-2 cells treated with *L. curvatus* BYB3+indole showed increased expression of the ZO-1 and claudin-1 proteins compared to cells treated with LPS alone (Figs. 4A and B). Furthermore, cells treated with the metabolites of BYB3+indole showed a significant increase in the expression of ZO-1 and claudin-1.

(A)

(B)
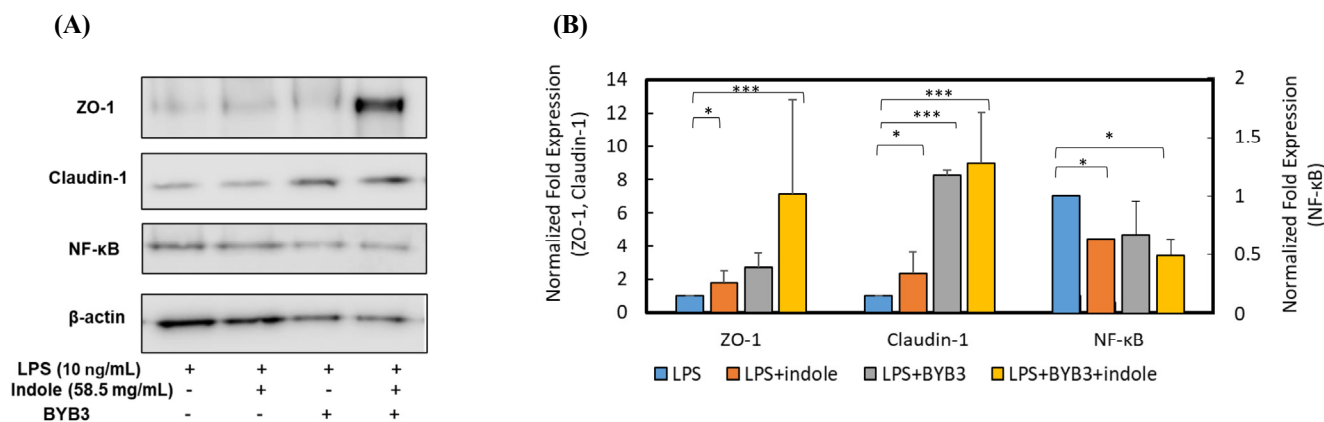
Fig. 4. Expression of TJ proteins and inflammatory responses. Caco-2 cells were co-treated with 10 ng/mL of LPS and indole, *Latilactobacillus curvatus* BYB3, and BYB3+indole for 24 h. Cells treated with LPS (10 ng/mL) alone served as the control. LPS down-regulated the expression of ZO-1 and claudin-1, increased paracellular permeability, and disrupted the epithelial membrane integrity (A). Protein expression was restored in the treatment groups. The metabolites of the *L. curvatus* BYB3+indole group showed the most significant increase in ZO-1 expression and a decrease in NF-κB expression. Graph (B) showed the ratios of the proteins ZO-1, claudin-1, and NF-κB, respectively, according to the β-actin calculated from the band density via western blots analysis (* $p<0.05$, ** $p<0.01$, *** $p<0.001$ compared with the control, n=3). ZO-1, zona occludens 1; NF-κB, nuclear factor-kappa B; LPS, lipopolysaccharide; TJ, tight junction.

To explore the anti-inflammatory effects of the metabolites on Caco-2 cells, alterations in NF-κB, a biomarker of inflammation, were examined. NF-κB p65 and the protein levels of total and phospho-p65 were detected by Western blot analysis. Compared to the LPS-treated cells (10 ng/mL, control), the Caco-2 cells treated with the supernatants of *L. curvatus* BYB3, indole, and metabolites of BYB3+indole showed decreased NF-κB expression. The reduction was significant in the presence of the metabolites of *L. curvatus* BYB3+indole. Interestingly, co-treatment with the metabolites of *L. curvatus* BYB3+indole and LPS had a remarkable effect on the attenuation of LPS-induced inflammation.
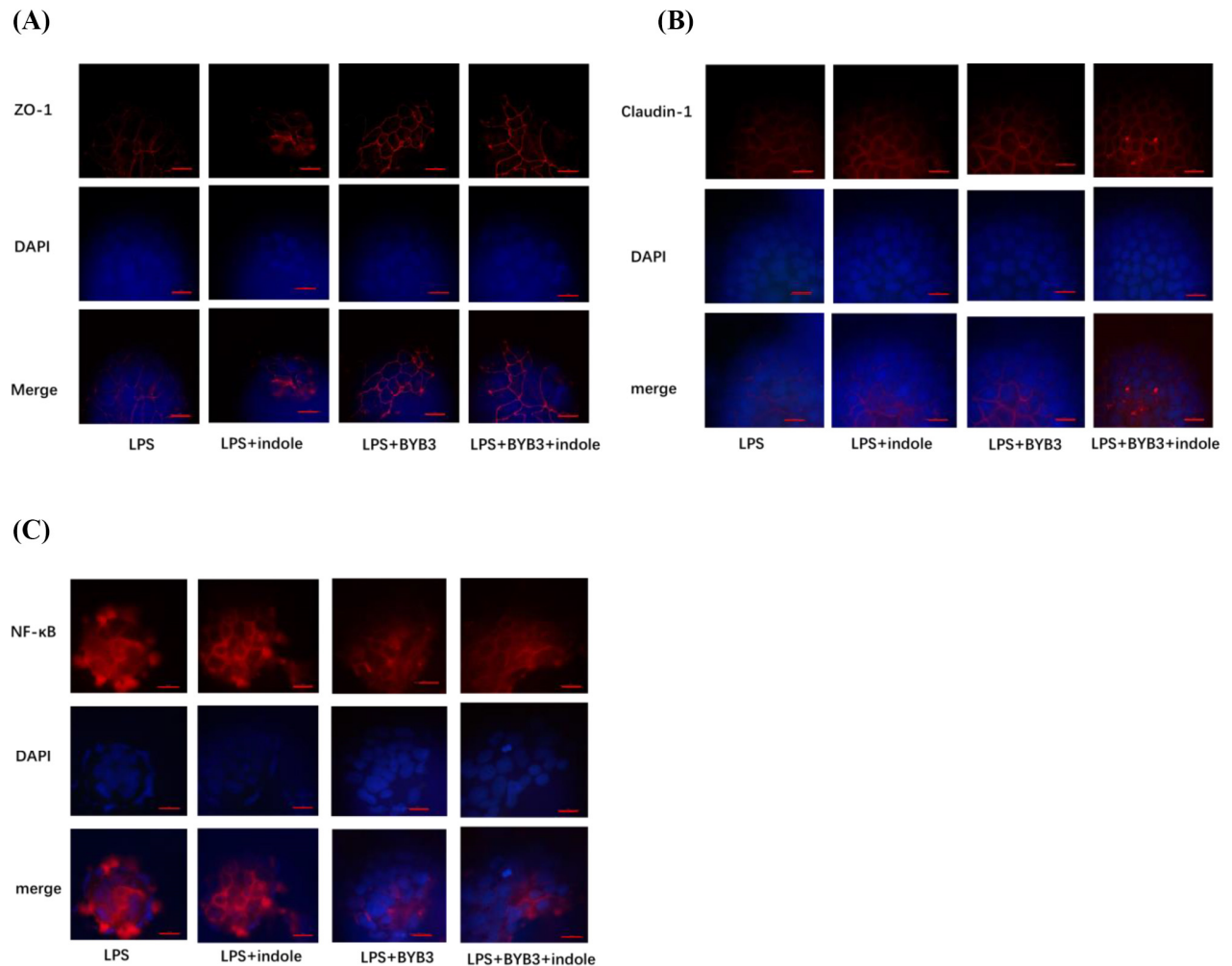
Immunofluorescence of the metabolites of *Latilactobacillus curvatus* BYB3 and indole

Immunofluorescence was used to detect the localization and expression of TJ proteins, as these results were more intuitive. The LPS-treated group showed severe disruption in the structure of TJ proteins structure (Fig. 5). In contrast, the TJ protein ZO-1 was intact without any damage in the cells treated with LPS+BYB3+indole. LPS-induced disruption was repaired in the LPS+indole, and LPS+BYB3 treated groups. Examination of claudin-1 expression revealed a trend similar to that observed for ZO-1 (Figs. 5A and B).

Consistent with this observation, immunofluorescence analysis of NF-κB demonstrated that p65 accumulated within the nucleus of Caco-2 cell monolayers treated with the metabolites of *L. curvatus* BYB3+indole. However, incubation with LPS decreased LPS-induced nuclear accumulation of NF-κB (Fig. 5C).

Identification and verification of indole compounds in the samples using high-performance liquid chromatography (HPLC)

HPLC analysis was performed to precisely identify and quantify indole derivatives. Several indole derivatives (100 μM each) were separated, and their peaks were detected by HPLC using a C-18 reverse column (Fig. 6). Under optimal conditions, the retention times of IAM, ILA, IAA, and indole were 13.2, 16.1, 19.3, and 29.1 min, respectively (Fig. 6A). The peak in Fig. 6B corresponds to the main components because of the presence of indole from the supernatants of the indole-

(A)

(B)

(C)

Fig. 5. Immunofluorescence of the localization and expression of TJ proteins. The supernatants of the indole and *Latilactobacillus curvatus* BYB3, and the metabolites of BYB3+indole treatment groups modulated the expression of (A) ZO-1, (B) claudin-1, and (C) NF-κB in differentiated Caco-2 cells exposed to an inflammatory stimulus. Caco-2 cells were differentiated and treated with 10 ng/mL of LPS (control) for 24 h. The control demonstrated severe disruption of the tight junction proteins. Co-treatment with supernatants of LPS, indole, and *L. curvatus* BYB3+indole improved the ZO-1 protein expression. However, the group treated with LPS and the metabolites of *L. curvatus* BYB3+indole displayed more improvement than those co-treated with LPS+indole and LPS+BYB3. (A) A similar trend was observed for the expression of claudin-1. (B) The metabolites of *L. curvatus* BYB3+indole suppressed the LPS-induced activation of NF-κB. (C) The reduction observed with the co-treatment of LPS+indole and LPS+BYB3 was lower than that observed in the group co-treated with LPS and metabolites of *L. curvatus* BYB3+indole (n=3). H&E stain, ×40. ZO-1, zona occludens 1; DAPI, 4',6-diamidino-2-phenylindole dihydrochloride; LPS, lipopolysaccharide; NF-κB, nuclear factor-kappa B; TJ, tight junction.

treated 0 h. The three peaks in Fig. 6C represent IAM, ILA, and indole. The main component in Fig. 6C, indicated by three peaks, including two of IAM and one of ILA, represented the supernatant of the *L. curvatus* BYB3 group fermented for 24 h. The indole content in the supernatants of the *L. curvatus* BYB3+indole group was reduced, and IAM and ILA metabolites were observed to varying degrees (Fig. 6D).

Discussion

Indole alleviates the symptoms of gastrointestinal disorders by activating the AhR (Hubbard et al., 2015). Several
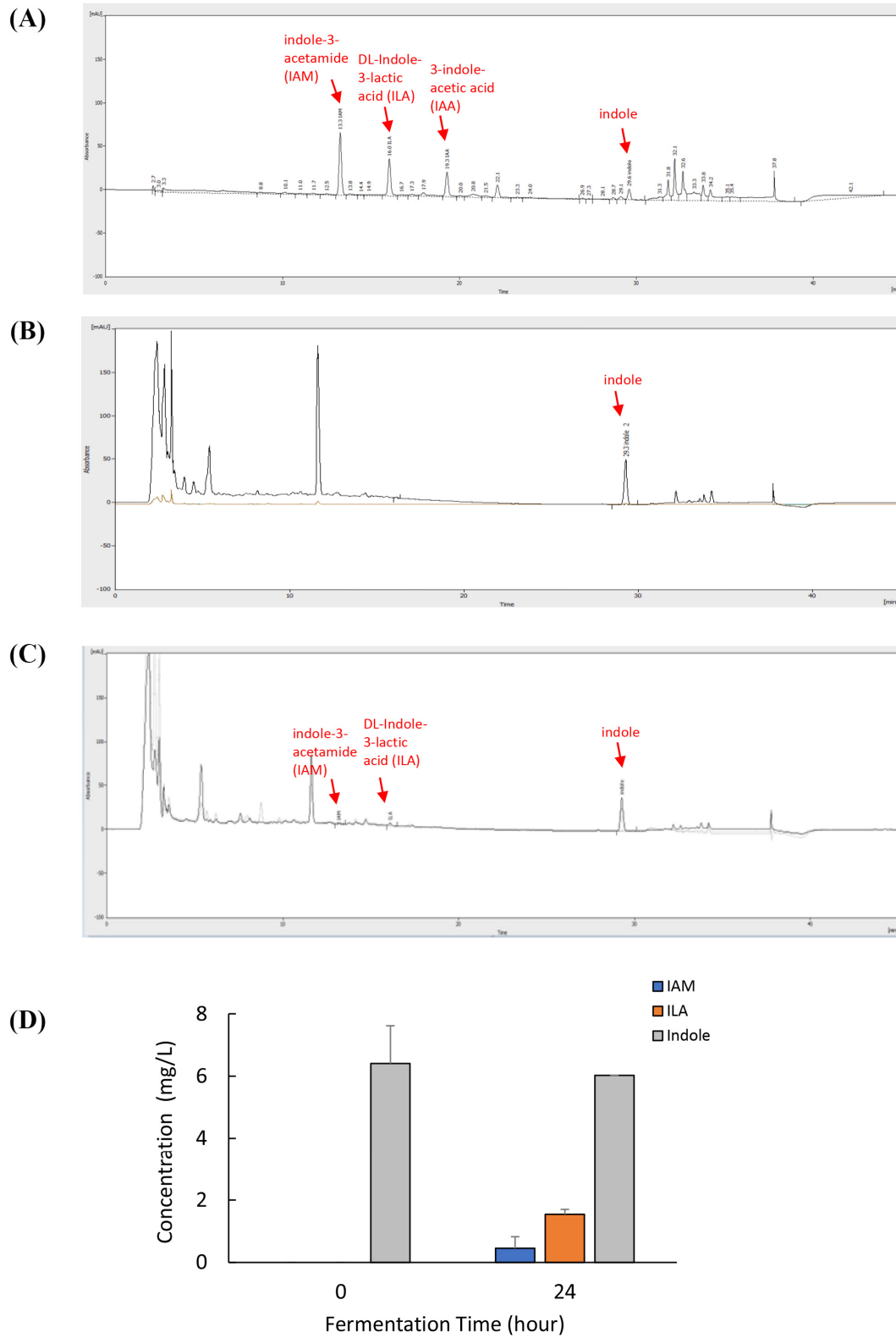
Fig. 6. HPLC chromatographs of samples' indole compounds. (A) Indole and indole derivates (ILA, IAA, and IAM) at 280 nm and UV spectra of 200–400 nm. (B, C) 0 and 24 h fermentation supernatants of *Latilactobacillus curvatus* BYB3+indole samples. (D) Indole and indole derivatives (ILA and IAM) in the supernatants of the 0 and 24 h fermentations of *L. curvatus* BYB3+indole samples (n=3). HPLC, high-performance liquid chromatography.

compounds have been proposed as putative endogenous AhR ligands, many of which are produced via pathways involved in the metabolism of tryptophan and indole, including indole-3-aldehyde, IAA, and many more (Bittinger et al., 2003; Chung and Gadupudi, 2011). In our previous study, AhR activation inhibited NF-κB expression, *in vivo* and *in vitro* (Salisbury and Sulentic, 2015). In macrophages, the activation of AhR signaling blocks NF-κB binding sites and masks NF-κB transcription activity, suppressing NLRP3 inflammasome activation (Huai et al., 2014). Hence, the current study aimed to identify the potential effect of metabolites of *L. curvatus* BYB3 and indole in mediating the recovery of TJ after LPS-induced disruption of the intestinal barrier in the colon mucosal cell layer. Our preliminary studies showed that *L. curvatus* BYB3 might play a role in alleviating inflammatory responses. However, the association between intestinal TJ proteins and inflammation influenced by *L. curvatus* BYB3 was not elucidated under *in vitro* conditions. The findings from this study suggest that the metabolites of *L. curvatus* BYB3 and indole can activate the AhR.

In previous studies, LPS-induced inflammation disrupted the integrity of IECs and increased paracellular permeability (Gao et al., 2017). The results from this study demonstrated that the supernatants of *L. curvatus* BYB3, indole, and metabolites of BYB3+indole inhibited LPS-induced inflammation in IECs by enhancing the expression of TJ proteins and decreasing paracellular permeability in Caco-2 cells. However, direct evidence is required to explore the association between the supernatants of cells treated with *L. curvatus* BYB3, indole, and the metabolites of *L. curvatus* BYB3+indole and intestinal permeability; such evidence was not available earlier. ZO-1, occludin, and claudin-1 are important TJ proteins that maintain permeability in the small intestine (Anderson and Van Itallie, 1995). Western blot analysis revealed that the administration of the metabolites of *L. curvatus* BYB3+indole significantly improved intestinal epithelial barrier function by increasing the expression of the TJ proteins ZO-1 and claudin-1. Deregulated NF-κB activation has been previously reported to contribute to the pathogenesis of various inflammatory diseases (Liu et al., 2017). In this study, the metabolites of BYB3+indole decreased NF-κB expression.

In a previous study, we determined that *Lactobacillus* improved the intestinal epithelial barrier function by increasing the expression of TJ proteins (Zeng et al., 2020). TEER is a commonly used indicator of intestinal epithelial membrane permeability (Srinivasan et al., 2015). An increase in the TEER and a decrease in paracellular permeability reflect the enhancement of the barrier function (Capaldo et al., 2017). The small intestine is one of the main organs of the digestive system, and the Caco-2 cell monolayer is a recognized intestinal cell line.

According to this study's HPLC analysis, only three indole compounds were detected among the metabolites of *L. curvatus* BYB3+indole, namely IAM, indole, and ILA. Several *Bacteroides* spp. and *Clostridium bartlettii* have been reported to produce ILA and IAA, whereas *Bifidobacterium* spp. have been reported to produce ILA (Aragozzini et al., 1979; Russell et al., 2013). However, there are few reports of *L. curvatus* producing ILA.

Our results provide evidence that microbiota-mediated metabolism inhibits LPS-induced inflammation, increasing the expression of TJ proteins. Based on the primary research results of this study, key metabolic molecules that improve intestinal should be investigated in further studies. We demonstrated that the metabolites of *L. curvatus* BYB3 and indole inhibited LPS-induced inflammation in IECs by enhancing TJs, which, in turn, reduced paracellular permeability. HPLC results confirmed that various concentrations of indole and indole derivatives (ILA and IAM) enhance TJ protein expression. This protective effect may provide a potential approach to restoring TJ barrier function, and AhR may be a novel therapeutic target in gut health and diseases such as IBD.

Conflicts of Interest

The authors declare no potential conflicts of interest.

Acknowledgements

Author Contributions

Conceptualization: Oh S. Data curation: Wang X, Yong CC, Oh S. Formal analysis: Wang X. Methodology: Wang X, Yong CC. Software: Wang X. Validation: Wang X, Yong CC. Investigation: Wang X, Yong CC. Writing - original draft: Wang X, Oh S. Writing - review & editing: Wang X, Yong CC, Oh S.

Ethics Approval

This article does not require IRB/IACUC approval because there are no human and animal participants.

References

Anderson JM, Van Itallie CM. 1995. Tight junctions and the molecular basis for regulation of paracellular permeability. Am J Physiol Gastrointest Liver Physiol 269:G467-G475.

Aragozzini F, Ferrari A, Pacini N, Gualandris R. 1979. Indole-3-lactic acid as a tryptophan metabolite produced by *Bifidobacterium* spp. Appl Environ Microbiol 38:544-546.

Arrieta MC, Madsen K, Doyle J, Meddings J. 2009. Reducing small intestinal permeability attenuates colitis in the Il10 gene-deficient mouse. Gut 58:41-48.

Behfarjam F, Jadali Z. 2018. Increased expression of aryl hydrocarbon receptor in peripheral blood mononuclear cells of patients with autoimmune hepatitis. Middle East J Dig Dis 10:105-108.

Bittinger MA, Nguyen LP, Bradfield CA. 2003. Aspartate aminotransferase generates proagonists of the aryl hydrocarbon receptor. Mol Pharmacol 64:550-556.

Capaldo CT, Powell DN, Kalman D. 2017. Layered defense: How mucus and tight junctions seal the intestinal barrier. J Mol Med 95:927-934.

Chung KT, Gadupudi GS. 2011. Possible roles of excess tryptophan metabolites in cancer. Environ Mol Mutagen 52:81-104.

Citi S. 2018. Intestinal barriers protect against disease. Science 359:1097-1098.

Esser C, Rannug A. 2015. The aryl hydrocarbon receptor in barrier organ physiology, immunology, and toxicology. Pharmacol Rev 67:259-279.

Gao Y, Li S, Wang J, Luo C, Zhao S, Zheng N. 2017. Modulation of intestinal epithelial permeability in differentiated Caco-2 cells exposed to aflatoxin M1 and ochratoxin a individually or collectively. Toxins 10:13.

Guo S, Al-Sadi R, Said HM, Ma TY. 2013. Lipopolysaccharide causes an increase in intestinal tight junction permeability *in vitro* and *in vivo* by inducing enterocyte membrane expression and localization of TLR-4 and CD14. Am J Pathol 182:375-387.

Guo S, Nighot M, Al-Sadi R, Alhmoud T, Nighot P, Ma TY. 2015. Lipopolysaccharide regulation of intestinal tight junction permeability is mediated by TLR4 signal transduction pathway activation of FAK and Myd88. J Immunol 195:4999-

5010.

Han Y, Zhao Q, Tang C, Li Y, Zhang K, Li F, Zhang J. 2020. Butyrate mitigates weanling piglets from lipopolysaccharide-induced colitis by regulating microbiota and energy metabolism of the gut–liver axis. Front Microbiol 11:588666.

Huai W, Zhao R, Song H, Zhao J, Zhang L, Zhang L, Gao C, Han L, Zhao W. 2014. Aryl hydrocarbon receptor negatively regulates NLRP3 inflammasome activity by inhibiting NLRP3 transcription. Nat Commun 5:4738.

Hubbard TD, Murray IA, Perdew GH. 2015. Indole and tryptophan metabolism: Endogenous and dietary routes to Ah receptor activation. Drug Metab Dispos 43:1522-1535.

Lee JH, Wood TK, Lee J. 2015. Roles of indole as an interspecies and interkingdom signaling molecule. Trends Microbiol 23:707-718.

Lee SH. 2015. Intestinal permeability regulation by tight junction: Implication on inflammatory bowel diseases. Intest Res 13:11-18.

Liu T, Zhang L, Joo D, Sun SC. 2017. NF-κB signaling in inflammation. Signal Transduct Target Ther 2:17023.

Marlowe JL, Fan Y, Chang X, Peng L, Knudsen ES, Xia Y, Puga A. 2008. The aryl hydrocarbon receptor binds to E2F1 and inhibits E2F1-induced apoptosis. Mol Biol Cell 19:3263-3271.

Neavin DR, Liu D, Ray B, Weinshilboum RM. 2018. The role of the aryl hydrocarbon receptor (AhR) in immune and inflammatory diseases. Int J Mol Sci 19:3851.

Odenwald MA, Turner JR. 2017. The intestinal epithelial barrier: A therapeutic target? Nat Rev Gastroenterol Hepatol 14:9-21.

Powell DN, Swimm A, Sonowal R, Bretin A, Gewirtz AT, Jones RM, Kalman D. 2020. Indoles from the commensal microbiota act via the AhR and IL-10 to tune the cellular composition of the colonic epithelium during aging. Proc Natl Acad Sci USA 117:21519-21526.

Russell WR, Duncan SH, Scobbie L, Duncan G, Cantlay L, Graham Calder A, Anderson SE, Flint HJ. 2013. Major phenylpropanoid-derived metabolites in the human gut can arise from microbial fermentation of protein. Mol Nutr Food Res 57:523-535.

Salisbury RL, Sulentic CEW. 2015. The AhR and NF-κB/rel proteins mediate the inhibitory effect of 2,3,7,8-tetrachlorodibenzo-p-dioxin on the 3' immunoglobulin heavy chain regulatory region. Toxicol Sci 148:443-459.

Sonowal R, Swimm A, Sahoo A, Luo L, Matsunaga Y, Wu Z, Bhingarde JA, Ejzak EA, Ranawade A, Qadota H, Powell DN, Capaldo CT, Flacker JM, Jones RM, Benian GM, Kalman D. 2017. Indoles from commensal bacteria extend healthspan. Proc Natl Acad Sci USA 114:E7506-E7515.

Srinivasan B, Kolli AR, Esch MB, Abaci HE, Shuler ML, Hickman JJ. 2015. TEER measurement techniques for *in vitro* barrier model systems. J Lab Autom 20:107-126.

Swimm A, Giver CR, DeFilipp Z, Rangaraju S, Sharma A, Ulezko Antonova A, Sonowal R, Capaldo C, Powell D, Qayed M, Kalman D, Waller EK. 2018. Indoles derived from intestinal microbiota act via type I interferon signaling to limit graft-versus-host disease. Blood 132:2506-2519.

Tlaskalová-Hogenová H, Štěpánková R, Hudcovic T, Tučková L, Cukrowska B, Lodinová-Žádníková R, Kozáková H, Rossmann P, Bártová J, Sokol D, Funda DP, Borovská D, Řeháková Z, Šinkora J, Hofman J, Drastich P, Kokešová A. 2004. Commensal bacteria (normal microflora), mucosal immunity and chronic inflammatory and autoimmune diseases. Immunol Lett 93:97-108.

Tsukita S, Furuse M, Itoh M. 2001. Multifunctional strands in tight junctions. Nat Rev Mol Cell Biol 2:285-293.

Turner JR. 2009. Intestinal mucosal barrier function in health and disease. Nat Rev Immunol 9:799-809.

Van Itallie CM, Anderson JM. 2006. Claudins and epithelial paracellular transport. Annu Rev Physiol 68:403-429.

Wang X, Li D, Meng Z, Kim K, Oh S. 2022. *Latilactobacillus curvatus* BYB3 isolated from kimchi alleviates dextran sulfate sodium (DSS)-induced colitis in mice by inhibiting IL-6 and TNF-R1 production. J Microbiol Biotechnol 32:348-354.

Wikoff WR, Anfora AT, Liu J, Schultz PG, Lesley SA, Peters EC, Siuzdak G. 2009. Metabolomics analysis reveals large effects of gut microflora on mammalian blood metabolites. Proc Natl Acad Sci USA 106:3698-3703.

Xie G, Peng Z, Raufman JP. 2012. Src-mediated aryl hydrocarbon and epidermal growth factor receptor cross talk stimulates colon cancer cell proliferation. Am J Physiol Gastrointest Liver Physiol 302:G1006-G1015.

Yang Z, Yu H, Tu H, Chen Z, Hu K, Jia H, Liu Y. 2022. Influence of aryl hydrocarbon receptor and sulfotransferase 1A1 on bisphenol AF-induced clastogenesis in human hepatoma cells. Toxicology 471:153175.

Yu M, Wang Q, Ma Y, Li L, Yu K, Zhang Z, Chen G, Li X, Xiao W, Xu P, Yang H. 2018. Aryl hydrocarbon receptor activation modulates intestinal epithelial barrier function by maintaining tight junction integrity. Int J Biol Sci 14:69-77.

Zeng Y, Zhang H, Tsao R, Mine Y. 2020. *Lactobacillus pentosus* s-pt84 prevents low-grade chronic inflammation-associated metabolic disorders in a lipopolysaccharide and high-fat diet c57/bl6j mouse model. J Agric Food Chem 68:4374-4386.

Zheng J, Wittouck S, Salvetti E, Franz CM, Harris HM, Mattarelli P, O'toole PW, Pot B, Vandamme P, Walter J, Watanabe K, Wuyts S, Felis GE, Gänzle MG, Lebeer S. 2020. A taxonomic note on the genus *Lactobacillus*: Description of 23 novel genera, emended description of the genus *Lactobacillus* Beijerinck 1901, and union of Lactobacillaceae and Leuconostocaceae. Int J Syst Evol Microbiol 70:2782-2858.